New Journal of Physics
The open access journal for physics

Probing the trapping and thermal activation dynamics of excitons at single twin defects in GaAs–AlGaAs core–shell nanowires

Daniel Rudolph[1], Lucas Schweickert[1], Stefanie Morkötter[1], Lukas Hanschke[1], Simon Hertenberger[1], Max Bichler[1], Gregor Koblmüller[1], Gerhard Abstreiter[1,2] and Jonathan J Finley[1,3]

[1] Physik Department, and Center of Nanotechnology and Nanomaterials, Walter Schottky Institut, Technische Universität München, Garching D-85748, Germany

[2] Institute for Advanced Study, Technische Universität München, Garching D-85748, Germany

E-mail: finley@wsi.tum.de

New Journal of Physics **15** (2013) 113032 (13pp)
Received 10 July 2013
Published 13 November 2013
Online at http://www.njp.org/
doi:10.1088/1367-2630/15/11/113032

Abstract. Time resolved and time-integrated photoluminescence (PL) spectroscopy is used to investigate the trapping and thermal activation dynamics of excitons bound to single twin defects in individual GaAs–AlGaAs core–shell nanowires. The GaAs core exhibits two distinct spectral emission features that are attributed to free and bound excitons. Time resolved measurements reveal lifetimes of $\tau_{FE} \sim 1.4$ ns and $\tau_{BE} \sim 4.0$ ns for the free and bound excitons, respectively. For temperatures above 30 K, the global PL intensity is quenched due to non-radiative carrier recombination. In contrast, for temperatures below 20 K we observe clear evidence for thermal detrapping of bound excitons into the continuum. By comparing the time-resolved PL spectra with a two-level rate equation model, quantitative values are obtained for both the exciton trapping and detrapping rates. Our data is consistent with a temperature independent exciton trapping rate >20 GHz that dominates the population dynamics of bound

[3] Author to whom any correspondence should be addressed.

Content from this work may be used under the terms of the Creative Commons Attribution 3.0 licence. Any further distribution of this work must maintain attribution to the author(s) and the title of the work, journal citation and DOI.

© IOP Publishing Ltd and Deutsche Physikalische Gesellschaft

excitons at $T = 6$ K. At elevated temperature, the detrapping rate is found to adhere to a thermally activated behavior characterized by a thermal activation energy of $E_A = 5.8 \pm 1.0$ meV, very close to the energy spacing of bound and free exciton emission features. This observation implies that bound excitons are thermally activated into the excitonic continuum without the need to overcome additional energetic barriers.

While most III–V semiconductors adopt a zincblende crystal structure in their bulk forms, III-As and III-P nanowires are often found to form mixed wurtzite/zincblende crystal structure or high densities of stacking faults under ambient conditions [1, 2]. Many groups have investigated the influence of growth parameters on the crystal structure of nanowires [3], with the goal of achieving crystal phase purity [4–12] or as a route to controllably modulate crystal structure [13–17]. The crystal phase mixing within nanowires alters the nanowire electronic and optical properties via a modification of the electronic band structure [18]. In most materials, the polytypic crystal structure leads to the formation of type-II heterostructures inducing a localization of electrons (holes) in zincblende (wurtzite) segments of the nanowire [18]. This charge carrier localization was found to dominate the electronic transport properties in InAs [19, 20] and InP [21] nanowires at low temperatures and has, for example, been used to produce electronic miniband-like effects in periodically modulated crystal nanowires [22].

The impact of crystal phase mixing on the optical properties of nanowires has been studied by various groups [16, 23–27]. The type-II band alignment was shown to produce PL features via recombination of spatially indirect excitons at wurtzite/zincblende heterointerfaces in InP [23, 24] and GaAs [25, 26] nanowires. These emission centers are localized along the nanowire axis and are typically red shifted with respect to the bandgap emission and have a longer lifetime [23–26]. For polytypic nanowires with predominant wurtzite structure, emission above the band gap energy of zincblende GaAs was reported [27]. Sufficiently small dimensions of the crystal phase segments lead to charge carrier confinement and, thus, to the formation of crystal phase quantum dots, that exhibit single photon emission [16]. While most existing work focuses on the impact of crystal structure on the energy and lifetime of photogenerated charge carriers, the trapping that leads to the localization of excitons is less studied. Recently, Graham *et al* [28] reported an S-shaped temperature dependence for the emission energy of localized excitons in polytypic GaAs nanowires and attributed the effect to thermally activated hopping of excitons into energetically more favorable crystal phase segments.

Here, we report investigations of trapping and thermal activation of excitons bound to single twin defects in individual GaAs–AlGaAs core–shell nanowires. We employ both time resolved and time-integrated PL spectroscopy to directly probe the luminescence dynamics and, thereby, the trapping and thermal activation dynamics of excitons localized at wurtzite/zincblende crystal phase boundaries. In a temperature range of 6–20 K, we observe PL dynamics, which evidence a thermal activation of bound excitons into the free exciton continuum. For a quantitative analysis of the exciton trapping and detrapping dynamics, we compare the time-resolved PL spectra with simulations according to a two-level rate equation model. This allows us to deduce a lower limit of 20 GHz for the exciton trapping rate, which dominates the exciton dynamics at low temperatures ($\sim$6 K). Upon increasing the lattice temperature, the detrapping rate is found to increase exponentially with a thermal

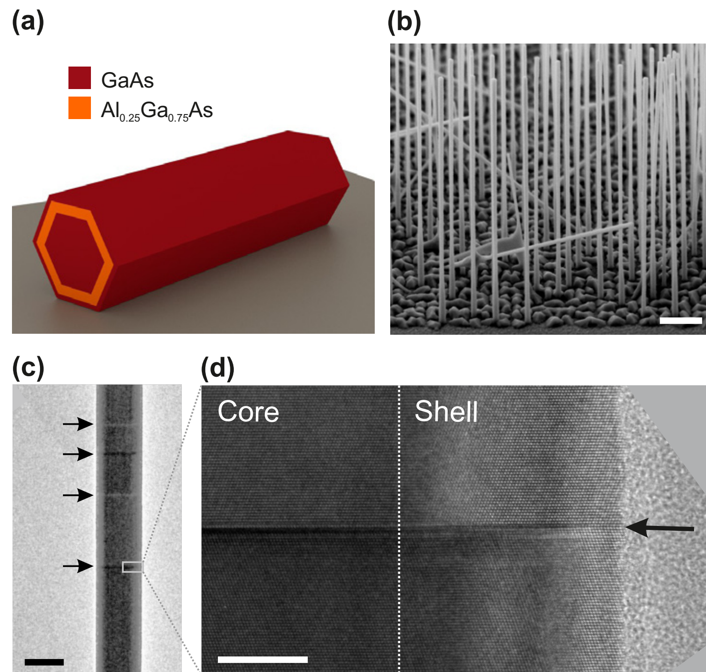

Figure 1. (a) Schematic representation of investigated nanowire heterostructure consisting of a GaAs core, AlGaAs shell and GaAs protection layer. (b) SEM micrograph of as-grown nanowires before transfer to Si templates for optical characterization. The scale bar is 1 μm. (c) TEM micrograph and (d) HRTEM detail of a single twin defect recorded from a GaAs–AlGaAs core–shell nanowire with a 24 nm-thick AlGaAs shell grown under similar growth conditions. A twinned zincblende crystal structure is found with an average twin defect density of $\sim$7 μm^{-1}. Arrows indicate the position of twin defects. The dashed line in (d) demarks the expected position of the core–shell interface. Twin defects are found to propagate from the nanowire core through the shell. The black (white) scale bar is 100 nm (10 nm).

activation energy of $E_A = 5.8 \pm 1.0$ meV. This value is in very good agreement with the energy spacing between free and bound exciton transitions and indicates, that bound excitons are thermally activated directly into the free exciton continuum without the need to overcome an additional energetic barrier. For $T > 30$ K, we find a degradation of the optical efficiency of the investigated nanowires due to non-radiative recombination.

We investigated GaAs–AlGaAs core–shell nanowires grown by molecular beam epitaxy (MBE) on SiO_2-coated Si(111) substrates. Growth templates were prepared by patterning thin ($\sim$20 nm) oxide masks using electron beam lithography as reported previously [29]. GaAs nanowires were synthesized in a Ga-catalyzed vapor–liquid–solid growth mode employing a substrate temperature of 610 °C, a Ga flux of 0.25 Å s^{-1} and an As flux of 1.03 Å s^{-1}. Figure 1(a) schematically depicts the structure of the investigated nanowires. To enhance their optical efficiency, GaAs nanowires were overgrown with an 8 nm thick $Al_{0.25}Ga_{0.75}As$ shell for surface passivation and a 4 nm GaAs protection layer to suppress oxidation of the AlGaAs shell. Further information on the growth of GaAs–AlGaAs core–shell nanowires can be found

in [30]. Figure 1(b) shows a typical scanning electron micrograph of the resulting nanowires with a length of $7.0 \pm 0.2\,\mu$m and diameters of 120–150 nm. The resulting nanowires exhibit a predominant zincblende crystal structure with occasional twin plane defects, as confirmed by Raman spectroscopy [31] and transmission electron microscopy (TEM): figures 1(c)–(d) depicts TEM micrographs of a representative GaAs–AlGaAs core–shell nanowire with a 24 nm-thick AlGaAs shell grown under similar growth conditions. Arrows in figure 1(c) indicate the position of individual twin defects, as evident from high resolution TEM (HRTEM) (cf figure 1(d)). In figure 1(d), the expected position of the core–shell interface is marked by a dashed line, which clearly illustrates, that twin defects propagate from the nanowire core through the AlGaAs shell. We find an average twin defect density of $\sim 7\,\mu\text{m}^{-1}$ along the nanowire axis. Besides individual twin defects, we do not observe elongated segments of WZ structure. In order to characterize individual nanowires using μ-PL spectroscopy, nanowires were dispersed onto Si (111) substrates and cooled to cryogenic temperatures in a He-flow cryostat. PL was collected along a direction perpendicular to the nanowire-axis after excitation with 4–6 ps duration laser-pulses at 1.59 eV (80 MHz repetition rate) focused using an NA = 0.5 objective onto the sample surface. Under these excitation conditions, the absorption length in GaAs is much larger than the nanowire diameter ($\sim$660 nm [32]), allowing us to probe the entire nanowire cross-section within the laser spot. The setup provides a laser spot size $<1\,\mu$m. The re-emitted light was collected by the same objective and spectrally filtered using a 0.5 m focal length monochromator (Princeton Instruments Acton, $1200\,\text{mm}^{-1}$ grating) and subsequently guided to a single photon avalanche diode (Perkin Elmer) for time-resolved detection.

Figure 2(a) shows a PL spectrum recorded from the center of a typical, individual nanowire at $T = 6$ K after excitation with a time-averaged power density of $250\,\text{W cm}^{-2}$. We observe emission in the energy range 1.500–1.515 eV. The strong asymmetry of the emission feature indicates contributions from two superimposed PL peaks. Indeed, the overall peak can be fitted by superposing two Gaussian peaks representing two excitonic states separated by $\Delta E = 4.8 \pm 0.3$ meV. This energy spacing corresponds closely to the localization energy of excitons at a single twin plane defect [26]. Twin defects represent a unit cell inclusion of wurtzite crystal phase in an otherwise zincblende matrix, and lead to the formation of indirect excitons with holes confined in the twin plane and electrons in the surrounding zincblende phase [25, 26]. In order to identify the origin of the two emission peaks we performed spectral and temporally resolved PL, an example of which is plotted in figure 2(b). Here, the circles correspond to data recorded after spectral filtering within a $\sim$0.7 meV bandwidth centered at 1.508 eV, while squares show data recorded around 1.502 eV. The data sets are normalized and offset for better comparison. At 1.508 eV, a clear mono-exponential decay transient is observed with a characteristic lifetime of $\tau \sim 1$ ns, consistent with literature for free excitons in GaAs nanowires [33]. The spectral position shows a small deviation from the expected literature value (1.515 eV [34]), an observation that we attribute to weak band bending effects arising from charge separation within the nanowire core [35]. In contrast to the mono-exponential dynamics observed at 1.508 eV, the time transient at 1.502 eV exhibits a clear bi-exponential character as indicated by the solid lines in figure 2(b). This is consistent with the spectral overlap of the two peaks at 1.502 eV as is entirely apparent from figure 2(a). In addition to the fast decay of the free exciton, a slow decay component is observed ($\tau \sim 4$ ns) and attributed to the low-energy state. Such an increased exciton lifetime is characteristic for the spatial separation of electron and hole at type-II heterointerfaces [25] and—in combination with the observed characteristic redshift—indicates that this peak stems from excitons localized at single twin plane defects.

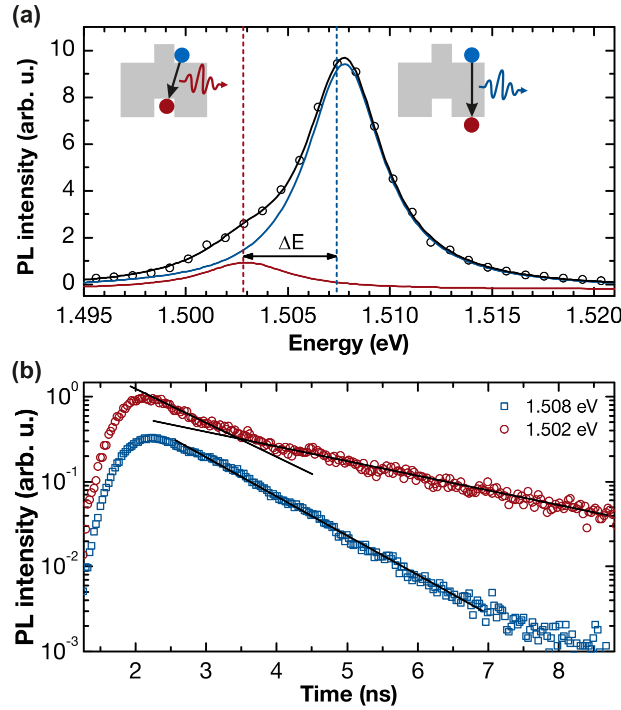

Figure 2. (a) PL spectrum recorded at $T = 6$ K from the center of an individual GaAs–AlGaAs core–shell nanowire. The asymmetric peak can be fitted (black line) with two Gaussian peaks separated by $\Delta E = 4.8 \pm 0.3$ meV as shown by the blue and red lines. (b) Time evolution of PL intensity recorded at $E = 1.502$ eV (red circles) and $E = 1.508$ eV (blue squares) as indicated by the dashed lines in panel (a). Data sets are offset for better comparison. The solid lines are guides to the eyes, clearly showing the bi-exponential nature of the decay transient at 1.502 eV. The fast decay is attributed to the recombination of free excitons while the slow decay is attributed to the recombination of indirect excitons localized at single twin plane defects.

We can rule out impurities and point defects as potential source of the low-energy PL feature, since those typically lead to a reduction of the carrier lifetime rather than a prolongation [36, 37].

In order to quantitatively analyze the observed charge carrier dynamics the observed time transients were fitted using a rate equation model. The structure of the model is depicted in the inset of figure 3(a), considering two distinct states for free and bound excitons with recombination rates Γ_{FE} and Γ_{BE}, respectively. The coupling between the two states is described by two additional rates Γ_{T} and Γ_{D} that phenomenologically describe the trapping of free excitons and detrapping of bound excitons, respectively. If the degeneracy of the bound exciton states is N_{D}, the time-dependent population of free and bound exciton populations are $N_{\mathrm{FE}}(t)$ and $N_{\mathrm{BE}}(t)$. These quantities satisfy the following rate equations:

$$\frac{\mathrm{d}N_{\mathrm{FE}}}{\mathrm{d}t} = -\Gamma_{\mathrm{FE}}N_{\mathrm{FE}} + \Gamma_{\mathrm{D}}N_{\mathrm{BE}} - \Gamma_{\mathrm{T}}N_{\mathrm{FE}}\left(1 - \frac{N_{\mathrm{BE}}}{N_{\mathrm{D}}}\right)$$

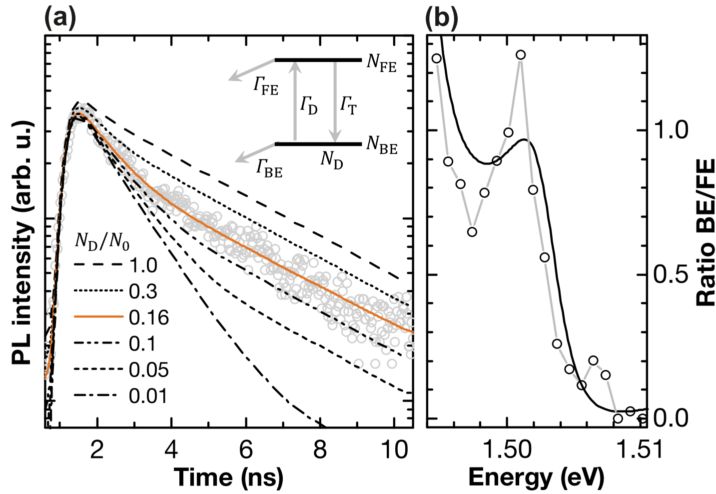

Figure 3. (a) Calculated time evolution of the PL intensity using the two-level rate-equation model described in the text. Solid (orange) line represents best fit to data recorded at $E = 1.502\,\text{eV}$. In addition, dashed/dotted lines display calculated decays for varying degeneracies of the low-energy state N_D given in units of N_0, the overall number of excitons at $t = 0\,\text{s}$.The inset shows a schematic representation of the applied rate-equation model as discussed in the text. (b) Energy dependence of the fitting parameter r, defined as the ratio of slow to fast decay. Solid line represents the ratio obtained from the quotient of the respective peak fits in figure 2(a). The overall good agreement validates the applied model.

and

$$\frac{dN_{BE}}{dt} = -\Gamma_{BE}N_{BE} - \Gamma_D N_{BE} + \Gamma_T N_{FE}\left(1 - \frac{N_{BE}}{N_D}\right).$$

This system of differential equations was solved numerically for the initial conditions $N_{FE}(t = 0\,\text{s}) = N_0$ and $N_{BE}(t = 0\,\text{s}) = 0$, i.e. assuming only a population of N_0 free excitons exists at $t = 0\,\text{s}$. Due to the non-resonant nature of the excitation this is likely to be a good description of the experimental situation. The overall PL intensity $I(t)$ recorded at energy E is then given by

$$I\,(t) = \frac{I_0\,(E)}{N_0}\,[N_{FE}\,(t - t_0) + r\,(E)\,N_{BE}\,(t - t_0)] + I_{BG},$$

where t_0 and I_{BG} are constants representing a time offset in our photon counting electronics and the background PL signal, $I_0(E)$ is the initial PL intensity at time $t = 0\,\text{s}$ and $r(E)$ is a parameter that represents the ratio of the intensities of the bound and free exciton peaks at the detection energy. The experimental data were fitted by iteratively calculating $I(t)$, convoluting the result with the instrument response function and minimizing the mean squared deviation of the resulting function from the data under variation of the fitting parameters. Importantly, most fitting parameters are global parameters that are independent of the PL energy (Γ_{FE}, Γ_{BE}, Γ_D, Γ_T, N_D), while only t_0, I_{BG}, r and I_0 were allowed to be energy dependent. Furthermore, the offset parameters t_0 and I_{BG} were found to exhibit no systematic dependence on E as expected.

Figure 3(a) again shows the time-resolved PL recorded at $T = 6\,\text{K}$ for $E = 1.502\,\text{eV}$ (circles) together with the best fit according to the model described above (solid line). It can

be seen that the fit provides a very good fit to the experimental data. The best fit was achieved for $N_D = (0.16 \pm 0.06)N_0$, $\Gamma_{FE} = 0.77 \pm 0.33$ GHz, $\Gamma_{BE} = 0.25 \pm 0.05$ GHz $\Gamma_T > 20$ GHz, $\Gamma_D <$ 1 GHz. For the trapping (detrapping) rate, we can only specify a lower (upper) limit since variations beyond this value have insignificant impact on fit quality. The rates above correspond to a trapping time <50 ps, a detrapping time >1 ns and lifetimes of 1.3 ± 0.4 and 4.0 ± 0.8 ns for free and bound excitons, respectively. As discussed above, the obtained values for the exciton lifetimes are in excellent agreement with literature values [25, 38]. Also, a trapping time in the picosecond-regime is fully consistent with literature values for other semiconductors [39, 40] and indicates, that in our case the process is also mediated by acoustic phonon emission [40]. The value obtained for N_D implies, that the bound exciton state is fully occupied by ~16% of the total number of excitons generated during one excitation pulse for the particular power density employed. In addition to the best fit, figure 3(b) also shows calculated PL decays for different values of the normalized degeneracy factor N_D/N_0 as dashed/dotted lines. It can be seen, that small variations of N_D lead to large discrepancies between calculation and best fit values. The limiting cases are also consistent with the physical expectations; for $N_D \to 0$ all excitons are forced into the free exciton continuum and the decay has purely mono-exponential character, as expected, with the fast recombination time of free excitons. In contrast, for $N_D \to N_0$ all generated excitons can occupy the bound excitation state and the decay, thus, becomes mono-exponential with the slower recombination time characteristic for indirect excitons. To furthermore validate the employed model, figure 3(b) shows the best-fit values of r as a function of the PL energy E (circles). Per definition, we expect r to directly reflect the ratio of free exciton to bound exciton contribution caused by the spectral overlap of the two PL peaks. The solid line in figure 3(b) represents the quotient of bound exciton to free exciton peak as obtained from the Gaussian fits to the time-integrated PL measurement depicted in figure 2(a). Indeed, we observe an excellent agreement between fitting parameter and the expected behavior. These observations confirm that the model developed provides a reliable description of the physics of the observed system and is well suited to the quantitative analysis of the experimental data.

In order to study the effect of temperature on the charge carrier dynamics, we recorded time-resolved PL spectra while changing the lattice temperature in the range $T = 6$–30 K. Below 10 K, temperature steps of $\Delta T = 1$ K were chosen, while for $T > 10$ K the step size was increased to 2 K. We acquired PL decays after spectral filtering within a bandwidth of ~0.7 meV, employing an integration time of 30 s. On the energy scale, a step size of 1 meV was employed. Figures 4(a)–(c) show representative time-resolved PL spectra for temperatures of 6, 10 and 18 K, respectively. The two exciton states can clearly be identified in this illustration by their different decay times. Centered around 1.508 eV, we observe the fast free exciton decay, while the slower bound exciton decay is centered around 1.502 eV, as indicated by the respective dashed lines in figures 4(a)–(c). With increasing temperature, the bound exciton emission becomes increasingly quenched, while the free exciton emission does not exhibit strong temperature dependence. This observation is in accord with expectations for thermal detrapping of bound excitons. We continue to quantitatively analyze these expectations utilizing the model discussed above. Figures 4(d)–(f) show the time evolution of PL as extracted from figures 4(a)–(c) at energy $E = 1.508$ eV for $T = 6$, 10 and 18 K, respectively (circles). In all cases, the decay is dominated by a single time constant. Besides a marginal decrease in overall PL intensity the three decay curves remain insensitive to the lattice temperature. To place this observation on a quantitative footing, the decay curves were fitted with the rate equation model for all temperatures, assuming all fitting parameters to be functions of the

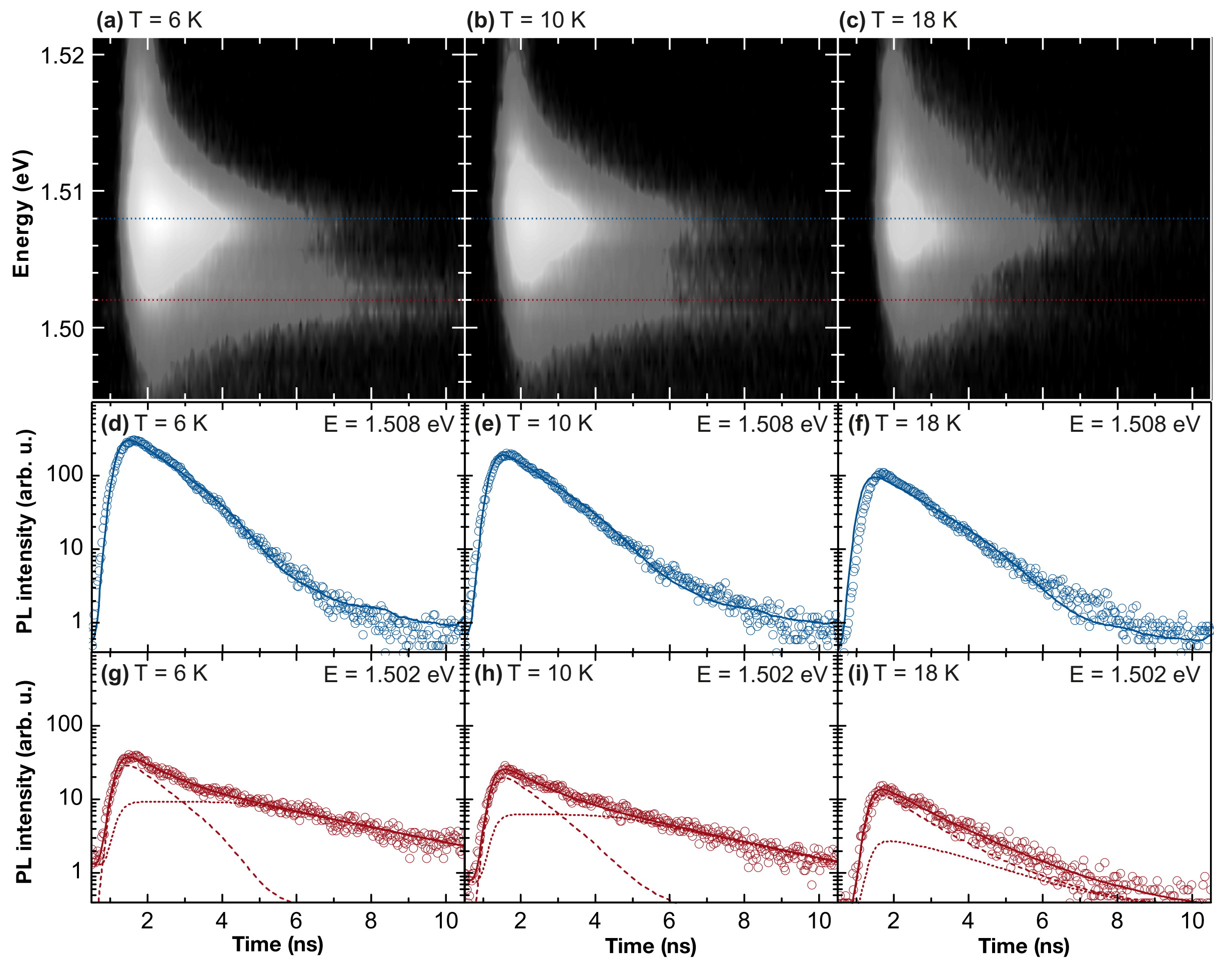

Figure 4. Time-resolved PL spectra recorded at three different sample temperatures: (a) $T = 6\,\mathrm{K}$, (b) $T = 10\,\mathrm{K}$ and (c) $T = 18\,\mathrm{K}$. Bright (dark) regions correspond to high (low) PL intensity, plotted on a logarithmic scale. With increasing temperature, a reduction of the slower decay centered around $E = 1.502\,\mathrm{eV}$ is observed. PL decay as detected at energy $E = 1.508\,\mathrm{eV}$ (circles) and calculated fits (solid lines) for different sample temperatures: (d) $T = 6\,\mathrm{K}$, (e) $T = 10\,\mathrm{K}$ and (f) $T = 18\,\mathrm{K}$. The time evolution is dominated by the fast recombination of free excitons and hardly depends on temperature. PL decay at $E = 1.502\,\mathrm{eV}$ (circles) and calculated fits (solid lines) for different sample temperatures: (g) $T = 6\,\mathrm{K}$, (h) $T = 10\,\mathrm{K}$ and (i) $T = 18\,\mathrm{K}$. The time evolution features contributions from both fast free exciton decay (dashed line) and slow bound exciton decay (dotted line). With increasing temperature, a quenching of the slow decay is observed due to thermally activated detrapping of bound excitons.

lattice temperature T. The solid lines in figures 4(d)–(f) depict the best fits to the experimental data. As expected, the offset parameters t_0, I_{BG} and the degeneracy of the bound exciton state $N_{\mathrm{D}}/N_0 = 0.15 \pm 0.03$ were found to be independent of T. Also r shows no trend with temperature—only statistical variations around the mean value $r = 0.011 \pm 0.003$. The small

value of r supports the initial observation that emission from the bound excitons play a negligible role in this spectral window, but is two orders of magnitude weaker than the contribution of free excitons. This small amplitude of the bound exciton contribution also implies, that the obtained values for Γ_{BE}, Γ_D and Γ_T are subject to larger errors due to their strong dependence on the occupancy of the bound exciton state. The free exciton lifetime, however, can be precisely determined from the fits. It is also found to be constant in the investigated temperature range with an average value of $\tau_{FE} = 1.4 \pm 0.2$ ns. This temperature-independent free exciton lifetime is consistent with earlier findings in GaAs heterostructures [41] and indicates, that exciton dissociation into free electron–hole pairs plays a negligible role in the investigated temperature range. Figures 4(g)–(i) show the PL decay recorded after spectral filtering at $E = 1.502$ eV as extracted from figures 4(a)–(c) for $T = 6$, 10 and 18 K (circles). Again, best fits to the data according to our model are depicted as solid lines. During the fitting procedure, the parameters Γ_{FE}, Γ_T and N_D were fixed to the values obtained from fitting the PL decay at $E = 1.508$ eV as shown in figures 4(d)–(f) and discussed above. In contrast to the PL decay curves at $E = 1.508$ eV, the contributions of the free and bound exciton state are on the same order of magnitude allowing us to study the trapping and detrapping dynamics in more detail. The dashed and dotted lines in figures 4(g)–(i) depict the separated contributions of free and bound exciton state, respectively. For $T = 6$ K, the bound state is populated via rapid exciton trapping until saturation. Since the trapping rate is much higher than the detrapping rate, the bound exciton state stays fully occupied as long as the overall number of excitons exceeds its degeneracy. Recombining bound excitons are immediately replaced by excitons trapped from the free exciton continuum. Only for $t > 5$ ns, when the overall decay has emptied the free exciton continuum, does the bound exciton state start to be depopulated with the lower recombination rate Γ_{BE}. In total, this behavior leads to the observed time-evolution of the total PL with a rapid decay in the beginning and a retarded decay for longer time delays after excitation.

However, this characteristic low temperature behavior is found to be strongly influenced by the lattice temperature T. As can be seen from figures 4(g)–(i) the relative intensity of the bound exciton becomes visibly quenched with increasing T. This confirms the initial observation of thermal exciton detrapping. Furthermore, the decay dynamics of free and bound exciton state change drastically. While at low temperatures bound and free exciton states depopulate with distinct rates $\Gamma_{BE} < \Gamma_{FE}$, for $T = 18$ K both states decay with similar rates in-between the low-temperature limits $\Gamma_{BE} < \Gamma_{i,j} < \Gamma_{FE}$. This indicates an increased detrapping rate as can be understood when looking at the limiting case of ultrafast coupling of the two exciton states. If we assume trapping and detrapping to occur on time scales much faster than the radiative recombination times, the occupancy of states will always obey thermal equilibrium. Each perturbation by a recombining exciton is immediately compensated for by a rapid redistribution of excitons via (de)trapping. As a result, the depopulation of both levels occurs with a common time constant Γ, representing an average of the two rates Γ_{BE} and Γ_{FE}, weighted by the equilibrium occupancy of the respective exciton levels.

For a more quantitative analysis of the temperature-dependent charge carrier dynamics, figure 5(a) shows the integrated PL intensity recorded at $E = 1.508$ eV for temperatures in the range of $T = 6$–110 K (squares). The overall intensity is found to be constant for temperatures below 30 K. Only for $T > 30$ K, we observe a rapid quenching of the PL intensity indicating the onset of thermally activated non-radiative recombination. The solid line depicts a fit to the data according to the model proposed by Williams and Eyring [42] for the temperature

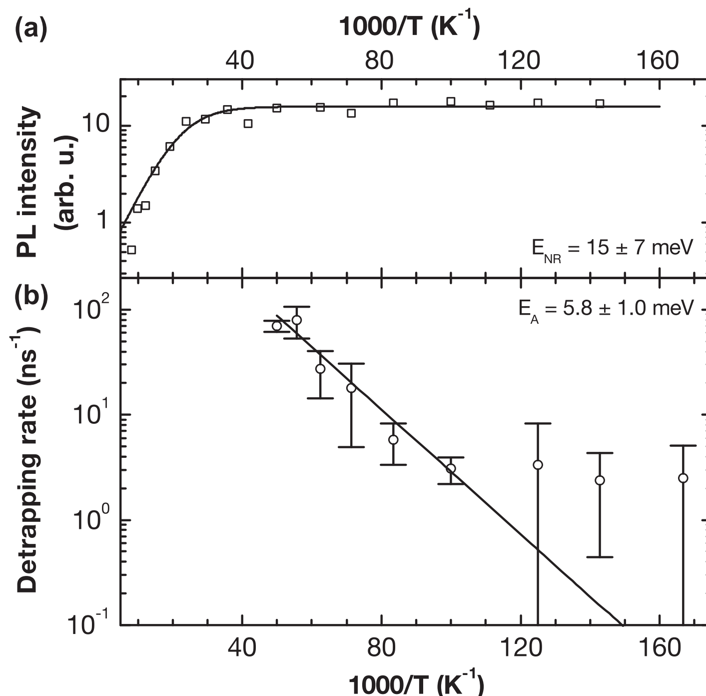

Figure 5. (a) Integrated PL intensity recorded at $E = 1.508\,\mathrm{eV}$ for different temperatures in the range from $T = 7$ to 110 K. The intensity quenches for $T > 30\,\mathrm{K}$ with an activation energy of $E_{\mathrm{NR}} = 15 \pm 7\,\mathrm{meV}$. Below 30 K, however, the PL intensity remains constant, indicating, that non-radiative processes are negligible in this temperature range. (b) Temperature dependence of the detrapping rate as obtained from fits to the time-resolved PL spectra. The thermal activation behavior was fitted assuming a Boltzmann factor dependence of the form $\Gamma_{\mathrm{A}} \propto \exp(-E_{\mathrm{A}}/kT)$ (solid line). An activation energy of $E_{\mathrm{A}} = 5.8 \pm 1.0\,\mathrm{meV}$ can be extracted from the fit, in very good agreement with the energy spacing between the two exciton levels $\Delta E = 4.8 \pm 0.3\,\mathrm{meV}$.

dependence of luminescence efficiency. It assumes a thermal activation into a metastable state that leads to non-radiative recombination and describes the temperature-dependent PL intensity by $I(T) = \frac{I_0}{1+C\exp(-E_{\mathrm{NR}}/kT)}$, where I_0 and C are fitting constants, k is the Boltzmann constant and E_{NR} is the activation energy of the non-radiative decay channel. The best fit to our data yields $E_{\mathrm{NR}} = 15 \pm 7\,\mathrm{meV}$. Our observations are in excellent agreement with earlier results by Titova *et al* [43], who measured the temperature-dependent PL intensity of GaAs–AlGaAs core–shell nanowires and found a quenching for $T > 50\,\mathrm{K}$ with an activation energy of 17 meV. In particular, this result proves the insignificance of non-radiative processes in the investigated temperature range of 6–20 K and justifies that our model includes solely radiative recombination.

The exciton detrapping rate as a function of lattice temperature is plotted in figure 5(b). It was obtained from fitting the PL decay transients recorded in the energy range 1.500–1.503 eV, where contributions from free and bound excitons are approximately equal (cf figure 2(b)) and the overall signal amplitude is sufficiently large to obtain reliable fitting results (cf figure 2(a)). Following the results discussed above, we assume the following fitting

parameters to be temperature-independent; the bound state degeneracy N_D, the spectral overlap ratio r, the radiative recombination rates Γ_{FE}, Γ_{BE}. The trapping rate Γ_T is also assumed to be temperature independent based on earlier results by O'Neil *et al* [39], in which a very weak temperature-dependence of the exciton trapping rate was observed with an only two-fold enhancement for an increase of temperature from $T = 4.8$ to 100 K [39]. Thus, we allowed only the detrapping rate Γ_D, the PL intensity I_0 and the offset parameters t_0, I_{BG} to vary with temperature. All other parameters were fixed to the values obtained from fitting the PL decay recorded at $T = 6$ K. In particular, the values of the parameters Γ_{FE}, Γ_{BE}, Γ_T and N_D, which are independent of the PL energy, were adopted from the fits in figures 4(d) and (g). The data points presented in figure 5(b) are each averaged over four sets of fits in the energy range of 1.500–1.503 eV with the error bars representing the standard deviation. For temperatures above 20 K, the contribution of bound excitons to the overall PL decay is already reduced to an extent that inhibits the deduction of a reliable value for the detrapping rate. In the observable temperature range, however, we find an enhancement of the detrapping rate by a factor of 30 upon increasing the temperature from 6 to 20 K. This trend furthermore reflects the temperature dependence of the Boltzmann factor, viz. $\Gamma_D(T) = A\exp(-E_A/kT)$ with A being a fitting constant and E_A representing the activation energy of the thermally activated detrapping process. The best fit to the data is plotted in figure 5(b) as a solid line and yields $E_A = 5.8 \pm 1.0$ meV. Within the experimental error, this value matches the energy spacing of bound and free exciton state, $\Delta E = 4.8 \pm 0.3$ meV, indicating that no energetic barrier needs to be overcome to detrap bound excitons, but excitons are directly activated into the free exciton continuum.

In conclusion, we have studied the temperature dependent dynamics of excitons in individual GaAs–AlGaAs core–shell nanowires by time-resolved PL spectroscopy. For high temperatures above 30 K, non-radiative recombination was found to result in a strong quenching of the PL intensity. For lower temperatures, two contributions to the PL emission were identified by their distinct time evolution: a fast radiative recombination of free excitons ($\tau_{FE} \sim 1.4$ ns) and a slower radiative recombination at lower energies caused by indirect excitons localized at single twin defects ($\tau_{BE} \sim 4.0$ ns). Comparison with a two-level rate equation model allowed us to study trapping and detrapping of excitons quantitatively. For $T = 6$ K the dynamics are dominated by rapid exciton trapping within $\sim$50 ps. While the experimental data can be explained with temperature-independent recombination and trapping rates, the detrapping rate is found to depend on temperature sensitively. Increasing T from 6 to 20 K increases the detrapping rate by a factor of 30 and leads to a depopulation of the bound exciton state via thermal activation into the free exciton continuum. An activation energy of $E_A = 5.8 \pm 1.0$ meV was found for this process in very good agreement with the energetic spacing between free and bound exciton states. The thermal detrapping of localized excitons is expected to not only influence the optical emission of polytypic nanowires, but also their transport behavior at low temperatures.

Acknowledgments

The authors thank A W Holleitner and P Weiser for SEM support and K Müller for PL experiment support and M Döblinger (Ludwig-Maximilians-Universität München, Department of Chemistry) for provision of TEM facilities and support. This work was funded by the Marie Curie FP7 Reintegration grant (Christina Totté, project officer), the EU FP7 project SOLID, the

DFG excellence program Nanosystems Initiative Munich, and the collaborative research center SFB 631. Further support was provided by the Technische Universität München, Institute for Advanced Study, funded by the German Excellence Initiative.

References

[1] Koguchi M, Kakibayashi H, Yazawa M, Hiruma K and Katsuyama T 1992 Crystal structure change of GaAs and InAs whiskers from zinc-blende to wurtzite type *Japan. J. Appl. Phys.* **31** 2061–5

[2] Hiruma K, Yazawa M, Katsuyama T, Ogawa K, Haraguchi K, Koguchi M and Kakibayashi H 1995 Growth and optical properties of nanometer-scale GaAs and InAs whiskers *J. Appl. Phys.* **77** 447

[3] Caroff P, Bolinsson J and Johansson J 2011 Crystal phases in III–V nanowires: from random toward engineered polytypism *Sel. Top. Quantum Electron.* **17** 829–46

[4] Joyce H J, Wong-Leung J, Gao Q, Tan H H and Jagadish C 2010 Phase perfection in zinc blende and wurtzite III–V nanowires using basic growth parameters *Nano Lett.* **10** 908–15

[5] Krogstrup P, Popovitz-Biro R, Johnson E, Madsen M H, Nygård J and Shtrikman H 2010 Structural phase control in self-catalyzed growth of GaAs nanowires on silicon (111) *Nano Lett.* **10** 4475–82

[6] Shtrikman H, Popovitz-Biro R, Kretinin A, Houben L, Heiblum M, Bukała M, Galicka M, Buczko R and Kacman P 2009 Method for suppression of stacking faults in wurtzite III–V nanowires *Nano Lett.* **9** 1506–10

[7] Shtrikman H, Popovitz-Biro R, Kretinin A and Heiblum M 2009 Stacking-faults-free zinc blende GaAs nanowires *Nano Lett.* **9** 215–9

[8] Hoang T B, Moses A F, Zhou H L, Dheeraj D L, Fimland B O and Weman H 2009 Observation of free exciton photoluminescence emission from single wurtzite GaAs nanowires *Appl. Phys. Lett.* **94** 133105

[9] Paiman S *et al* 2009 The effect of V/III ratio and catalyst particle size on the crystal structure and optical properties of InP nanowires *Nanotechnology* **20** 225606

[10] Dick K A, Caroff P, Bolinsson J, Messing M E, Johansson J, Deppert K, Wallenberg L R and Samuelson L 2010 Control of III–V nanowire crystal structure by growth parameter tuning *Semicond. Sci. Technol.* **25** 024009

[11] Mohseni P K and LaPierre R R 2009 A growth interruption technique for stacking fault-free nanowire superlattices *Nanotechnology* **20** 025610

[12] Johansson J and Karlsson L 2008 Effects of supersaturation on the crystal structure of gold seeded III–V nanowires *Cryst. Growth Des.* **9** 766–73

[13] Algra R E, Verheijen M A, Borgström M T, Feiner L-F, Immink G, Van Enckevort W J P, Vlieg E and Bakkers E P A M 2008 Twinning superlattices in indium phosphide nanowires *Nature* **456** 369–72

[14] Dick K A, Thelander C, Samuelson L and Caroff P 2010 Crystal phase engineering in single InAs nanowires *Nano Lett.* **10** 3494–9

[15] Caroff P, Dick K and Johansson J 2008 Controlled polytypic and twin-plane super lattices in III–V nanowires *Nature Nanotechnol.* **4** 50

[16] Akopian N, Patriarche G, Liu L, Harmand J-C and Zwiller V 2010 Crystal phase quantum dots *Nano Lett.* **10** 1198–201

[17] Rieger T, Lepsa M I, Schäpers T and Grützmacher D 2013 Controlled wurtzite inclusions in self-catalyzed zinc blende III–V semiconductor nanowires *J. Cryst. Growth* **378** 506–10

[18] Murayama M and Nakayama T 1994 Chemical trend of band offsets at wurtzite/zinc-blende heterocrystalline semiconductor interfaces *Phys. Rev.* B **49** 4710

[19] Schroer M D and Petta J R 2010 Correlating the nanostructure and electronic properties of InAs nanowires *Nano Lett.* **10** 1618–22

[20] Thelander C, Caroff P, Plissard S, Dey A and Dick K 2011 Effects of crystal phase mixing on the electrical properties of InAs nanowires *Nano Lett.* **11** 2424–9

[21] Wallentin J, Ek M, Wallenberg L R, Samuelson L and Borgström M T 2012 Electron trapping in InP nanowire FETs with stacking faults *Nano Lett.* **12** 151–5

[22] Ikonic Z, Srivastava G and Inkson J 1993 Electronic properties of twin boundaries and twinning superlattices in diamond-type and zinc-blende-type semiconductors *Phys. Rev.* B **48** 17181

[23] Bao J, Bell D C, Capasso F, Wagner J B, Mårtensson T, Trägårdh J and Samuelson L 2008 Optical properties of rotationally twinned InP nanowire heterostructures *Nano Lett.* **8** 836–41

[24] Pemasiri K *et al* 2009 Carrier dynamics and quantum confinement in type II ZB–WZ InP nanowire homostructures *Nano Lett.* **9** 648–54

[25] Spirkoska D *et al* 2009 Structural and optical properties of high quality zinc-blende/wurtzite GaAs nanowire heterostructures *Phys. Rev.* B **80** 1–9

[26] Heiss M *et al* 2011 Direct correlation of crystal structure and optical properties in wurtzite/zinc-blende GaAs nanowire heterostructures *Phys. Rev.* B **83** 1–10

[27] Jahn U, Lähnemann J, Pfüller C, Brandt O, Breuer S, Jenichen B, Ramsteiner M, Geelhaar L and Riechert H 2012 Luminescence of GaAs nanowires consisting of wurtzite and zinc-blende segments *Phys. Rev.* B **85** 045323

[28] Graham A M, Corfdir P, Heiss M, Conesa-Boj S, Uccelli E, Fontcuberta i Morral A and Phillips R T 2013 Exciton localization mechanisms in wurtzite/zinc-blende GaAs nanowires *Phys. Rev.* B **87** 125304

[29] Hertenberger S, Rudolph D, Bichler M, Finley J J, Abstreiter G and Koblmüller G 2010 Growth kinetics in position-controlled and catalyst-free InAs nanowire arrays on Si(111) grown by selective area molecular beam epitaxy *J. Appl. Phys.* **108** 114316

[30] Rudolph D *et al* 2013 Spontaneous alloy composition ordering in GaAs–AlGaAs core–shell nanowires *Nano Lett.* **13** 1522–7

[31] Zardo I, Conesa-Boj S, Peiro F, Morante J R, Arbiol J, Uccelli E, Abstreiter G and Fontcuberta i Morral A 2009 Raman spectroscopy of wurtzite and zinc-blende GaAs nanowires: polarization dependence, selection rules, and strain effects *Phys. Rev.* B **80** 245324

[32] Sturge M D 1962 Optical absorption of gallium arsenide between 0.6 and 2.75 eV *Phys. Rev.* **127** 768–73

[33] Perera S *et al* 2008 Nearly intrinsic exciton lifetimes in single twin-free GaAs/AlGaAs core–shell nanowire heterostructures *Appl. Phys. Lett.* **93** 053110

[34] Grilli E, Guzzi M, Zamboni R and Pavesi L 1992 High-precision determination of the temperature dependence of the fundamental energy gap in gallium arsenide *Phys. Rev.* B **45** 1638–44

[35] Caface R A, Guimarães F E G, Arakaki H, De Souza C A and Pusep Y A 2013 Photoluminescence of radial heterostructured GaAs/AlGaAs/GaAs nanowires *J. Appl. Phys.* **113** 064315

[36] Dumke W P 1963 Optical transitions involving impurities in semiconductors *Phys. Rev.* **132** 1998–2002

[37] Nelson R J and Sobers R G 1978 Minority-carrier lifetimes and internal quantum efficiency of surface-free GaAs *J. Appl. Phys.* **49** 6103

[38] ‘t Hooft G W, Van der Poel W A J A, Molenkamp L W and Foxon C T 1987 Giant oscillator strength of free excitons in GaAs *Phys. Rev.* B **35** 8281–4

[39] O’Neil M, Marohn J and McLendon G 1990 Picosecond measurements of exciton trapping in semiconductor clusters *Chem. Phys. Lett.* **168** 208–10

[40] Bastard G, Delalande C, Meynadier M, Frijlink P and Voos M 1984 Low-temperature exciton trapping on interface defects in semiconductor quantum wells *Phys. Rev.* B **29** 7042–4

[41] Hjalmarson H P, Gilliland G D, Wolford D J, Kuech T F and Bradley J A 1994 Temperature-dependent radiative recombination of free excitons in high-quality GaAs heterostructures *J. Lumin.* **60–61** 830–3

[42] Williams F E and Eyring H 1947 The mechanism of the luminescence of solids *J. Chem. Phys.* **15** 289

[43] Titova L V, Hoang T B, Jackson H E, Smith L M, Yarrison-Rice J M, Kim Y, Joyce H J, Tan H H and Jagadish C 2006 Temperature dependence of photoluminescence from single core–shell GaAs–AlGaAs nanowires *Appl. Phys. Lett.* **89** 173126